High-performance biofuel cell made with hydrophilic ordered mesoporous carbon as electrode material

*Chun Xian Guo[1], Feng Ping Hu[1], Xiong Wen Lou, Chang Ming Li**

School of Chemical and Biomedical Engineering, Nanyang Technological University, Singapore 637457, Singapore
* Corresponding author. Tel.: +65 67904485; fax: +65 67911761.
E-mail address: ecmli@ntu.edu.sg (C.M. Li).
[1] Both the authors have equal contributors in this work.

ABSTRACT

A highly hydrophilic ordered mesoporous carbon has been synthesized by a microwave assisted method from a mixture containing glucose and poly(vinyl alcohol) and with a silica template to have high hydrophilicity, low charge transfer resistance and large specific surface area. The new carbon material is further used as an electrode material to fabricate an anode-limited glucose/O_2 biofuel cell, which gives an output power density of 110 μW cm^{-2} with cell voltage of 0.72 V, a performance much higher than the reported anodes made from SWNT, bi-polymer layer and carbon black at the same or even higher glucose concentration. This work provides a universal approach to synthesize functional carbon nanomaterials with desired architectures and properties for various important applications in energy conversion systems such as fuel cells and solar cells.

Keywords:

Biofuel cells; Electrode material; Hydrophilicity; Ordered mesoporous carbon; Microwave irradiation

1. Introduction

Enzymatic biofuel cells (BFCs) as a renewable energy system employ enzymes to harvest electrical energy from biofuels [1–4]. Distinctly from the conventional H_2/O_2 fuel cells, BFCs can use biofuels while working under moderate conditions, such as mild medium and ambient temperature, thus becoming a very attractive green energy system [5,6]. Moreover, since fuels consumed by BFCs, such as glucose and oxygen, are generally rich in a biological system, BFCs can be used as the required energy systems for implantable drug delivery and autonomous health monitoring systems [7–9]. These amazing properties and important potential applications have attracted great interest in the fundamental study and development of BFCs. Recently, one of the significant advances of BFCs is development of biocathodes and/or bioanodes with direct electron transfer ability of enzymes [10–12]. Direct electron transfer, a direct electrochemistry process can significantly improve the energy conversion efficiency of a bioenergy system. It can also eliminate the use of additional electron transfer mediators, which suffer from fast loss thus resulting in high operation expense and large overpotential. Unfortunately, direct electron transfer of enzymes with bare electrode is very difficult [13–15]. It is mainly caused by the deeply buried redox centers of enzymes in their insulating shell and also by denature of the enzymes on electrode surfaces.

Functional nanomaterials could provide an electron-mediating function to facilitate the direct electron transfer of enzymes by reducing the electron tunneling distance between their active sites and electrode surface [2,16–20]. Recently, carbon nanomaterials, such as multi-walled carbon nanotubes (MWNT), single-walled carbon nanotubes (SWNT), graphene, $C_{60,}$ carbon black and hollow carbon spheres, have been attracted increasing attentions because of their good conductivity, chemical inertness, and relatively wide potential window. Some of these well-known carbon materials have also shown their capability to facilitate direct electron transfer of proteins with electrodes such as MWNT for hemoglobin [21], SWNT for microperoxidase MP-11 [22], and graphene for glucose oxidase (GOD) [23]. However, it still remains a great challenge to further enhance the direct electron transfer rate of enzymes, eventually resulting in high-performance biofuel cells.

Ordered mesoporous carbons (OMCs) have been recently developed as a new class of carbon nanomaterials with high specific surface area, uniform pore distribution, high thermal/mechanical stability and flexible framework composition [24–26]. OMCs could also be a good candidate to achieve fast direct electron transfer of enzymes, but they exhibit rather unreactive surface and hydrophobic property due to lack of oxygen-containing functional groups caused by the high carbonization temperature during synthesis [26,27]. The poor surface reactivity and hydrophobicity not only make it difficult for immobilization of enzymes, but also seriously prohibits the reactant from solution to access the active sites of the enzymes on the electrode surface [28]. Clearly, this drawback is one of the main barricades for the direct electron transfer at an enzyme/electrode interface and high-performance bioufuel cells.To make their surface active, a number of methods have been explored by using super strong oxidation agents such as nitric acids and ozone for producing some oxygenated functionalities. Unfortunately, these functional methods always result in damage of pore and surface structure to deteriorate the electrocatalytic performance [29,30].

Microwave irradiation with superior capability in providing a high reaction rate and increased yield of products, is a noninvasive and clean process to synthesize a variety of materials [31,32], and has been recently applied to make carbon related nanomaterials including carbon nanotubes, hollow carbon nanospheres and core/shell metal/carbon nanoparticles [33,34], demonstrating its great potential to tailor carbon nanomaterials with unique physicochemical properties and structures. In this work, we report a microwave assisted approach to prepare highly hydrophilic OMC material by incorporating a suitable polymer in the synthesis. Meanwhile, direct electron transfer of an enzyme on the carbon material was investigated. Furthermore, an anode-limited glucose/O_2 biofuel cell was developed and its performance was explored.

2. Experimental

2.1. Synthesis of carbon materials

In preparation of the carbon material, 1 g of molecular sieve SBA-15 (Jilin University High-Tech. Co. Ltd., Changchun, China) was immersed in a solution containing 1.25 g of glucose, 0.14 g of sulphuric acid and 5 g water. The mixture was drying by placing in an oven for 6 h at 373 K, followed by increasing the temperature to 433 K and maintaining for 6 h. The carbonization was

conducted with different times in a microwave oven (LG, MS-2744B, 1000W) using graphite as the heat-conducting layer, which has been widely used in carbonizations [35,36]. The heating procedure was 2 min on and 2 min off, since it resulted in uniform due to eliminating the overheating. It was observed that during the on-off pulse heating the on-cycle was longer than 2 min or the off-cycle less than 2 min, sparks of the samples occurred due to overheating, resulting in extremely non-uniform products with dark color on the heat-contacting layer while very light color in the center part. The carbonization was further optimized for the cycle times. With one cycle of 2 min on and 2 min off, the product exhibited mixed grey and white colors, indicating an uncompleted carbonization. After two-cycle heating, a uniformly black sample was obtained, showing a completed carbonization. However, when 3 heating cycle was implemented, the product turned to partially white color, clearly indicating burned carbon. The carbon/silica composite produced by the microwave oven was washed with 5 wt% hydrofluoric acid at room temperature to remove the silica template. The silica-free product was finally obtained by filtering followed by washing with ethanol and drying at 393 °K. To synthesize the polymer-added carbon material, the same procedure was used but with the precursor solution containing 0.9 g of glucose and 0.35 g of poly(vinyl alcohol) (PVA, M_w 13,000–23,000, Sigma) from the beginning. For comparison, regular mesoporous carbon was also synthesized by the conventional method at 900°C under N_2 flow for 3 h.

2.2. Preparation of enzyme electrodes

Glassy carbon electrodes (GCE, 3mm in diameter, CH Instruments Inc., USA) were polished to a mirror-like finish sequentially with 1.0, 0.3, and 0.05 μm alumina slurry followed by rinsing with deionized water. The electrodes were successively sonicated in 1:1 nitric acid, acetone and deionized water, and then were dried at room temperature. Enzyme (glucose oxidase), from *Aspergillus niger*, Sigma–Aldrich) immobilization was achieved by immersing 25mg of the material in 2.5 mL of glucose oxidase solution (10mg mL^{-1}, pH 7.0, 0.01 M phosphate buffered saline (PBS)) under ambient conditions and shaking for half an hour, and then stored at 4°C overnight. The maximum protein loadings on as-prepared carbons with and without PVA determined by Ultraviolet–visible (UV–vis) spectra at 280nm were 38wt% and 32wt% respectively. The mixture was then centrifuged and 2 mL of 0.01 M, pH 7.0, PBS was added. The glucose oxidase-immobilized carbons were reshaken and 5 μL of this suspension was deposited on the centre of the pretreated GCE, which was then left to dry at room temperature. Then 3 μL of 0.5% nafion aqueous solution (to fix the protein-impregnated material) were applied on electrode surface, which was covered with a plastic tube and left to dry overnight. For electrodes without glucose oxidase, the same procedures were used except the solution used is pure 0.01 M PBS.

2.3. Construction of biofuel cell

The biofuel cell consisted of two custom-fabricated plastic cabinets with 6.0cm length, 6.0cm width and 5.0cm height, which was separated by a Nafion membrane (Aldrich). Electrodes were designed by using enzyme/carbon modified GCE electrode (3mm in diameter) as the anode and Pt wire (2 mm in diameter and 30 mm length) as the cathode. The anode was placed in one cabinet containing 10mM glucose in 0.1 M PBS (pH 7.0) and the cathode was in the other cabinet containing 0.1 M PBS (pH 1.0, adjusted by H_2SO_4).

2.4. Material characterizations and biofuel cell measurement

Morphology and microstructure of materials were examined by field emission scanning electron microscopy (FESEM, JSM-6700F, Japan). Transmission electron microscopy (TEM) images were obtained using JEOL JEM-2100F transmission electron microscope operated at 200 kV. Nitrogen adsorption/desorption experiments were carried out at 77.3 K by an Autosorb-1 (Quantachrome Instruments) analyzer. Water contact angle was measured by FTA1000C Class (First Ten Angstroms, USA). Fourier transform infrared (FTIR, Bruker EQUINOX 55 DuroscopeTM ATR) spectra were recorded with a resolution of 1 cm^{-1}. Electrochemical measurements (cyclic voltammograms and electrochemical impedance spectroscopy) were performed in a three-electrode cell using CHI-760B electrochemical station (CH Instruments Inc., USA) with the modified GCE electrode, Pt wire and Ag/AgCl as working, counter and reference electrodes, respectively. Performance of the biofuel cell was characterized by external resistance loads and the output voltage was measured by a multimeter. Before measurement, the biofuel cell was allowed to equilibrate for 1 h before data collection.

3. Results and discussions

The synthesis routes of two carbon materials are outlined in Scheme 1. Three steps are required for both carbon materials. First, carbon precursor (glucose for OMC-1; glucose and polymer PVA for OMC-2) is impregnated into silica template. Second, the silica/carbon precursor composite is treated by mild heating. Third, carbonization is completed with intermittent microwave irradiation and a unique mesoporous carbon material is obtained by removing the silica template. PVA is selected as the added in polymer because of its high water-solubility for an aqueous preparation process and abundant hydroxyl groups for high hydrophilicity. The microstructure and morphology of as-prepared carbon materials were studied by FESEM as shown in Fig. 1. The low magnifications of Fig. 1a and c illustrate that both carbon materials have rod-like morphology with a relatively uniform size, similar to the morphology of the silica template SBA-15 reported [26]. The high-resolution FESEM images in Fig. 1b and d show that the carbon rods are composed by arrayed dense parallel channels.

The detail structures of the two carbon materials were further investigated by TEM. The representative TEM images of both carbon materials are illustrated in Fig. 2. The relatively bright lines are images of pore structures of carbon, while the black lines are the carbon scaffold. The low TEM images of OMC-1 in Fig. 2a and OMC-2 in Fig. 2c display that both carbon materials have high porosity. The high-magnification TEM image of OMC-1 in Fig. 2b clearly demonstrates the detailed pore structure. The pores of OMC-1 are arranged in an ordered manner with diameter around 3.6 nm and the centers of adjacent pores 10 nm apart, which are in agreement with the replica structure of the SBA-15 [26]. In comparison of the pore diameter of OMC-1 with the wall-thickness of SBA-15 reported, we can find that the pore diameter of the former is a little larger than that of the later. It is possibly caused by the carbon materials slightly shrank during the microwave treatment, which has been also observed in carbon materials synthesized by conventional methods [37]. The detailed pore structure of OMC-2 in Fig. 2d shows similar structure as OMC-1, clearly demonstrating that the microwave irradiation approach can produce ordered mesoporous carbon materials similar to the conventional high-temperature/vacuum method and the incorporated polymer during synthesis does not affect the ordered pore structure.

Representative nitrogen adsorption/desorption isotherms of the synthesized carbon materials and their corresponding pore-size distributions obtained from analysis of the desorption branch using the BJH (Barett–Joyner–Halenda) method are shown in Fig. 3a and c, indicating that both carbon materials have the pore-size distribution centered at 3.6 nm. The pore-size distributions are consistent with the TEM observations in Fig. 2, which further confirms the formation of a mesoporous structure. The Brunauer-Emmett-Teller (BET) area, a specific surface area of OMC-1 and OMC-2 obtained from the nitrogen adsorption are 475 m^2g^{-1} (curve 1) and 821.8 m^2g^{-1} (curve 2) respectively. The difference of the specific surface area is likely mainly contributed from micropores, which have significant effect on the BET surface area of a porous material [38]. In comparison of the pore-size distribution in microporous (less than 2 nm) regions (Fig. 3c) for both materials, it is revealed that there is a clear pore-size distribution centered around 1 nm for OMC-2, while not obvious for OMC-1. The only difference between the two synthesis routes for both carbon materials is the polymer PVA addition in the preparation of OMC-2. A reasonable speculation is that PVA has low burning point than that of largely cross-linked glucose [39], and a part of PVA might be burned during microwave irradiation, which resulted in micropores centered on 1 nm for OMC-2. Though the exact mechanism for OMC-2 with more micropores is still not very clear, these results demonstrate that this microwave irradiation method can produce mesoporous carbons with uniform pore structure and the addition of a suitable polymer during the synthesis can result in higher specific surface area. The nitrogen adsorption–desorption isotherm and corresponding pore size distribution of the OMC prepared by the conventional method [24,26] are given in Fig. 3b and d, respectively. The pore-size distribution is centered at 4.0 nm, a slightly larger size than that of OMC-2 of 3.6 nm. The BET area obtained from the nitrogen adsorption for conventionally synthesized OMC is around 820 $m^2\ g^{-1}$, which is similar to that of OMC-2 synthesized by the microwave heating. However, the microwave heating needs only 8 min (2 min on and 2 min off, two cycles), and thus is significantly more efficient than the conventional method (under N_2 flow at 900°C for 3 h).

The hydrophilicity of the as-prepared carbon materials was evaluated by water contact angle measurements. The water contact angle of OMC-1 is 38.4° (Fig. 4a), which is much smaller than 79.1° observed for the ordered mesoporous carbon materials synthesized by the conventional method [26]. The water contact angle of OMC-2 shown in Fig. 4b exhibits an angle of 20.6°, which is even smaller than that of OMC-1 and quite close to that of PVA [40]. These observations could be explained by Fourier transform infrared (FTIR) spectra of both carbon materials shown in Fig. 5. The broad absorption bands centered at 3450 and 1620cm^{-1} correspond to the stretching and bending modes of the OH group, and the absorption bands at 1234 and 1385 cm^{-1} are assigned to the stretching and bending vibrations of C–OH. These bands could be found in both OMC-1 and OMC-2, indicating that the hydroxyl group still remains in the two carbon materials. Apparently, the hydroxyl group can improve hydrophilicity of the mesoporous carbons. The difference of the two carbon materials in the FTIR spectra lies in the relative band peak intensity. Clearly, the relative band peak intensity of OMC-2 is larger than that of OMC-1, showing that OMC-2 with more hydroxyl groups. This is why OMC-2 is more hydrophilic. These results indicate that this microwave irradiation method can synthesize highly hydrophilic carbon s and the hydrophilicity can be further improved by impregnation of a suitable polymer during synthesis.

The electrochemical properties of OMC-1 and OMC-2 were characterized by electrochemical impedance spectroscopy in 10mM $Fe(CN)6^{3-}/^{4-}$ to 1.0 M KCl. The measured impedance result is

displayed with real part (Z') on the *X*-axis and the imaginary part (Z'') on the *Y*-axis, known as Nyquist plot in Fig. 6, in which well-defined frequency-dependent semicircle impedance curves are observed at the high frequency range followed by a straight line. Randle equivalent circuit (inset of Fig. 6) is often used to model the complex impedance in an electrochemical cell, which is composed of the ohmic resistance of the electrolyte solution, R_s in connection in series with parallel elements of double layer capacitance, C_{dl}, and Faraday impedance, Z_f, which comprises serially connected charge-transfer resistance, R_{ct} and Warburg impedance, Z_w. The lower R_{ct} indicates the faster charge transfer rate between electrode and reactant species. The values of R_{ct} obtained from Fig. 6 are 17.5 and 5.2 $\Omega\,cm^2$ for OMC-1 and OMC-2 electrode, respectively, indicating that OMC-2 has much lower charge transfer resistance.

These mesoporous carbons were further explored as electrode material for direct electron transfer of enzyme. As mentioned in the experiment part, the measured percentage adsorption for glucose oxidase by UV–vis spectra at 280 nm is 38 and 32 wt% for OMC-2 and for OMC-1, respectively, which is not proportional to the BET area of OMCs (821.8 and 475 $m^2\,g^{-1}$ for OMC-2 and OMC-1, respectively). As we know, the dimensional size of proteins such as GOD ranges from 5 to 10 nm [41] such that the outside surface and part of pores (>5 nm) of OMCs might be utilized for GOD immobilization. However, it is recently reported that the small pores (<2 nm) could be a stoichiometric electron acceptor and host for a variety of electron-donating guest species [42,43]. Also as discussed above, good surface hydrophilicity is favorable for immobilization of enzymes and the reactant from solution to access the active sites of the enzymes on the electrode surface [28]. OMC-2 with large amount of micropores and good hydrophilicity might be useful in protein direct electron transfer. Cyclic voltammograms (CVs) were employed to study the possibility of direct electron transfer of GOD on OMC-2. Fig. 7a shows CVs of different electrodes in a N_2-saturated PBS buffer solution. Both GOD and OMC-2 modified electrodes alone only exhibit capacitive, squared CVs over the potential window caused by their double layer capacitance (curves 1 and 2). However, GOD/OMC-2 modified electrode shows a pair of well-defined redox peaks at −535 and −476 mV over its capacitive response, which is consistent with the reported redox potentials of FAD/$FADH_2$, the active center of GOD at neutral pH [13], thus clearly demonstrating the ability of direct electron transfer of GOD on OMC-2 electrode. Electrochemical behavior of GOD on OMC-1 was also studied and the result is illustrated in Fig. 7 (curve 4), from which a very weak redox peaks over its capacitive response can be found. The active enzyme density on the electrode surface (mol cm^{-2}) can be calculated through integrating the redox peaks at scan rate of 100 mVs^{-1} [13]. The calculated active enzyme density on OMC-2 is 3.2×10^{-10} mol cm^{-2}, which is much higher than that on OMC-1 (0.22×10^{-10} mol cm^{-2}). The measured percentage adsorption of 38 wt% for OMC-2 and 32 wt% for OMC-1 can be converted into a unit surface adsorption of 1.5×10^{-9} mol cm^{-2} for OMC-2 and 1.25×10^{-9} mol cm^{-2} for OMC-1. Thus, about 21% and 1.8% of the GOD immobilized on OMC-2 and OMC-1 retains the electrochemical activity, thus indicating that OMC-2 is a much better electrode material for direct electrochemistry of GOD. The effect of scan rate on electron transfer behavior of GOD on OMC-2 was also investigated. Both cathodic and anodic peak currents of CVs obtained are linearly proportional with scan rates from 50 to 250 mV s^{-1}, as shown in Fig. 7b, indicating that the redox reaction of immobilized GOD is a surface-controlled electrochemical process and further proving the direct electron transfer of GOD on OMC-2 material. The Laviron model [44] is often used to estimate the electron transfer rate constant K_s, from CV measurements. In the GOD/OMC-2 electrode, K_s is about 3.98 s^{-1}, which is much larger than K_s of GOD on SWNTs (0.3 s^{-1}) [45], MWNTs (1.53s^{-1}) [46], and gold nanoparticles (1.3s^{-1}) [47]. The results

clearly demonstrate that the enhanced direct electron transfer rate of GOD on the synthesized carbon material.

Glucose/O_2 biofuel cell was constructed with GOD/OMC-2 modified GCE electrode as the anode and Pt as the cathode, and the setup details can be found in the experiment part. The electrocatalytic behaviors of the anode and cathode were studied and the results are shown in Fig. 8. The catalytic electrooxidation of glucose on GOD/OMC-2 anode occurs at −0.6 V vs Ag/AgCl, and reaches its plateau of 150 μA cm^{-2} near −0.5 V vs Ag/AgCl. Due to GOD possesses direct electron transfer on OMC-2, the electrooxidation of the GOD towards glucose in the fuel cell is obviously direct electron transfer-based catalysis process. For cathode, catalytic electroreduction of O2 was observed at +0.6 V vs Ag/AgCl and reached its 1200 μA cm^{-2} near +0.4 V vs Ag/AgCl. Compared with the plateau current density of cathode, the smaller anode plateau current density indicates that the operation of this biofuel cell is anode-limited, which is essential to accurately evaluate the anode electrocatalytic performance.

The performance of the assembled glucose/O_2 biofuel cell was investigated. By using external resistance loads, the polarization and output power density against current density of the assembled biofuel cell are displayed in Fig. 9. The polarization curve shows that the open-circuit potential (OCP) was near 1.2 V and the cell voltage could keep around 0.7 V at current density from 50 to 150 μA cm^{-2} (current density was calculated versus geometric electrode area, giving 0.07 cm^2 for GCE with diameter 3mm). The plot of power density versus current density has a volcano shape, which is a typical relationship of output power density against the current density for fuel cells. The maximum power density is 110 Wcm^{-2}, which is obtained at a current density of 150 μA cm^{-2} with a cell voltage of 0.72 V. This maximum power density achieved at physiological glucose concentration (10mM) is much higher than that of glucose/O_2 biofuel cells with anodes made from OMC-1 (12.5 μW cm^{-2} at 0.58 V, 10mM glucose, data not shown), regular OMC synthesized by the conventional method (38.7 μWcm^{-2} at 0.54 V, the cell voltage around 0.7 V at current density from 45 μA cm^{-2}, 60mM glucose, reported in [48]), and other materials such as SWNT (9.5 μWcm^{-2} at 0.52 V, 30mM glucose) [5], bilayer polymer membrane (14.5 μWcm^{-2} at 0.36 V, 10mM glucose) [49], and carbon black (90 μWcm^{-2} at 0.4V, 10mM glucose) as well [50]. Since the performance of this biofuel cell is the anode-limited, the excellent output power density achieved at the same or even lower glucose concentration in this work over the reported works, should be ascribed to the superior electrocatalytic activity of the GOD immobilized on as-prepared carbon material.

4. Conclusion

In summary, a highly hydrophilic mesoporous carbon has been synthesized with a microwave method by incorporating a polymer during the synthesis. Glucose oxidase immobilized on the carbon exhibits fast direct electron transfer rate. An anode-limited glucose/O_2 biofuel cell based on the glucose oxidase functionalized carbon as the anode and a Pt wire as the cathode delivers output power density as high as 110 μWcm^{-2} at a cell voltage of 0.72V in a physiological environment, a performance much higher than that of SWNT, bi-polymer layer membrane and carbon black as the anode at the same or even higher glucose concentration. Considering its high power output, the new carbon-based biofuel cell promoted by the unique carbon material renders great potentials for practical applications. The strategy by introduction of a suitable polymer into

the microwave assisted synthesis can also be used to make other functional nanomaterials with desired architecture and specific properties.

Acknowledgement

The authors are grateful to the Asian Office of Aerospace Research and Development, Department of The Air Force of USA for the financial support to this work under contract of FA5209-05- P-0505.

References

[1] M.J. Cooney, V. Svoboda, C. Lau, G. Martin, S.D. Minteer, Energy Environ. Sci. 1 (2008) 320–337.
[2] S.C. Barton, J. Gallaway, P. Atanassov, Chem. Rev. 104 (2004) 4867–4886.
[3] S. Kerzenmachera, J. Ducréeb, R. Zengerlea, F. von Stettena, J. Power Sources 182 (2008) 1–17.
[4] I. Willner, Science 298 (2002) 2407–2408.
[5] Y.M. Yan, W. Zheng, L. Su, L.Q. Mao, Adv. Mater. 18 (2006) 2639–2643.
[6] R.L. Arechederraa, B.L. Treua, S.D. Minteer, J. Power Sources 173 (2007) 126–161.
[7] R.F. Service, Science 296 (2002) 1222–1224.
[8] A.K. Shukla, P. Suresh, S. Berchmans, A. Rajendran, Curr. Sci. 87 (2004) 455–468.
[9] Y. Qiao, C.M. Li, S.J. Bao, Q.L. Bao, J. Power Sources 170 (2007) 79–84.
[10] J.B. Kim, J.W. Grate, P. Wang, Trends Biotechnol. 26 (2008) 639–646.
[11] F. Davis, S.P.J. Higson, Biosens. Bioelectron. 22 (2007) 1224–1235.
[12] A. Zebdaa, L. Renaudb, M. Cretina, C. Innocenta, F. Pichotd, R. Ferrignob, S. Tingry, J. Power Sources 193 (2009) 602–606.
[13] S.J. Bao, C.M. Li, J.F. Zang, X.Q. Cui, Y. Qiao, J. Guo, Adv. Funct. Mater. 18 (2008) 591–599.
[14] A. Riklin, E. Katz, I. Willner, A. Stocker, A.F. Buckmann, Nature 376 (1995) 672–675.
[15] C.X. Guo, F.P. Hu, C.M. Li, P.K. Shen, Biosens. Bioelectron. 24 (2008) 819–824.
[16] V. Soukharev, N. Mano, A. Heller, J. Am. Chem. Soc. 126 (2004) 8368–8369.
[17] J.P. Liu, C.X. Guo, C.M. Li, Y.Y. Li, Q.B. Chi, X.T. Huang, L. Liao, T. Yu, Electrochem. Commun. 11 (2009) 202–205.
[18] W.J. Doherty, N.R. Armstrong, S.S. Saavedra, Chem. Mater. 17 (2005) 3652–3660.
[19] A.P. Borolea, S. LaBargeb, B.A. Spottb, J. Power Sources 188 (2009) 421–426.
[20] X.D. Shangguan, J.B. Zheng, Electroanalysis 21 (2009) 881–886.
[21] R.Y. Zhang, X.M. Wang, K.K. Shiu, J. Colloid Interface Sci. 316 (2007) 517– 522.
[22] J.J. Gooding, R. Wibowo, J.Q. Liu, W.R. Yang, D. Losic, S. Orbons, F.J. Mearns, J.G. Shapter, D.B. Hibbert, J. Am. Chem. Soc. 125 (2003) 9006–9007.
[23] C.S. Shan, H.F. Yang, J.F. Song, D.X. Han, A. Ivaska, L. Niu, Anal. Chem. 18 (2009) 2378–2382.
[24] S.H. Joo, S.J. Choi, I. Oh, J. Kwak, Z. Liu, O. Terasaki, R. Ryoo, Nature 412 (2001) 169–172.
[25] L. Calvilloa,M.J. Lázaroa, E. García-Bordejéa, R.Molinera, P.L.Cabotb, I. Esparbéb, E. Pastorc, J.J. Quintanac, J. Power Sources 169 (2007) 59–64.
[26] C.D. Liang, Z.J. Li, S. Dai, Angew. Chem. Int. Ed. 47 (2008) 3696–3717.
[27] H.I. Lee, J.H. Kim, D.J. You, J.E. Lee, J.M. Kim, W.S. Ahn, C. Pak, S.H. Joo, H. Chang, D. Seung, Adv. Mater. 20 (2008) 757–762.
[28] M.M. Titirici, A. Thomas, M. Antonietti, J. Mater. Chem. 17 (2007) 3412–3418.
[29] S. Wu, H.X. Ju, Y. Liu, Adv. Funct. Mater. 17 (2007) 585–592.
[30] Z.J. Li, W.F. Yan, S. Dai, Langmuir 21 (2005) 11999–12006.
[31] C.O. Kappe, Angew. Chem. Int. Ed. 43 (2004) 6250–6284.
[32] E.H. Hong, K.H. Lee, S.H. Oh, C.G. Park, Adv. Funct. Mater. 13 (2003) 961–966.
[33] K. Chen, C.L. Wang, D. Ma, W.X. Huang, X.H. Bao, Chem. Commun. (2008) 2765–2767.

[34] Y.L. Hsin, C.F. Lin, Y.C. Liang, K.C. Hwang, J.C. Horng, J.A.A. Ho, C.C. Lin, J.R. Hwu, Adv. Funct. Mater. 18 (2008) 2048–2056.
[35] S.Q. Song, Y. Wang, P.K. Shen, J. Power Sources 170 (2007) 46–49.
[36] C.L. Wang, D. Ma, X.H. Bao, J. Phys. Chem. C 112 (2008) 17596–17602.
[37] X. Zhuang, Y. Wan, C.M. Feng, Y. Shen, D.Y. Zhao, Chem. Mater. 21 (2009) 706–716.
[38] H.Y. Chen, H.X. Xi, X.Y. Cai, Y. Qian, Microporous Mesoporous Mater. 118 (2009) 396–402.
[39] N.N. Geng, C.M. Xiao, Chin. Chem. Lett. 20 (2009) 111–114.
[40] C.H. Kim, M.S. Khil, H.Y. Kim, H.U. Lee, K.Y. Jahng, Biomed. Mater. Res. B 78 B (2006) 283–290.
[41] Y.J. Wang, F. Caruso, Chem. Commun. (2004) 1528–1529.
[42] M. Vettraino, M.L. Trudeau, D.M. Antonelli, Adv. Mater. 12 (2000) 337–341.
[43] S. Sotiropoulou, V. Vamvakaki, N.A. Chaniotakis, Biosens. Bioelectron. 20 (2005) 1674–1679.
[44] E. Laviron, J. Electroanal. Chem. 101 (1979) 19–28.
[45] J.Q. Liu, A. Chou, W. Rahmat, M.N. Paddon-Row, J.J. Gooding, Electroanalysis 17 (2005) 38–46.
[46] C.X. Cai, J. Chen, Anal. Biochem. 332 (2004) 75–83.
[47] S. Zhao, K. Zhang, Y. Bai, W.W. Yang, C.Q. Sun, Bioelectrochemistry 69 (2006) 158–163.
[48] M. Zhou, L. Deng, D. Wen, L. Shang, L.H. Jin, S.J. Dong, Biosens. Bioelectron. 24 (2009) 2904–2908.
[49] F. Sato, M. Togo, M.K. Islam, T. Matsue, J. Kosuge, N. Fukasaku, S. Kurosawa, M. Nishizawa, Electrochem. Commun. 7 (2005) 643–647.
[50] A. Habrioux, K. Servat, S. Tingry, K.B. Kokoh, Electrochem. Commun. 11 (2009) 111–113.

List of Figures

List of Scheme

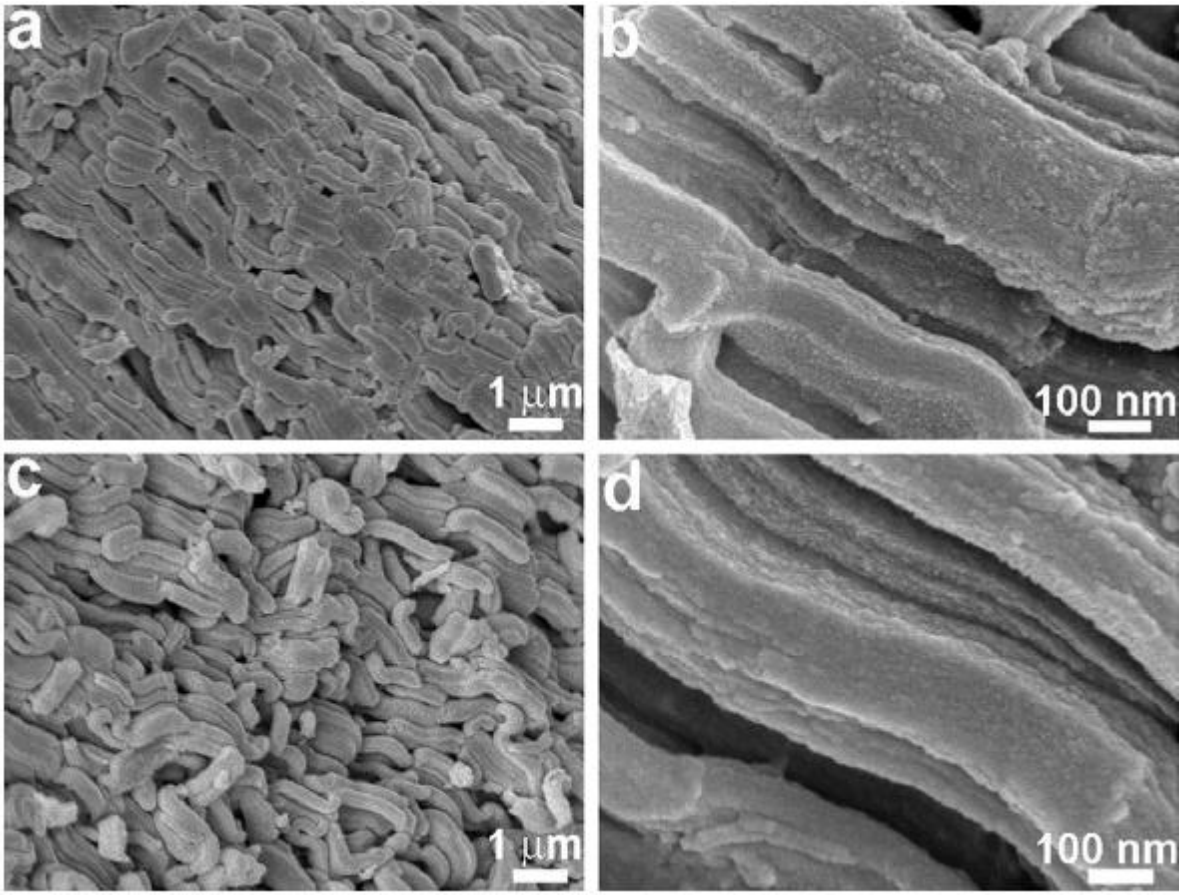

Figure 1

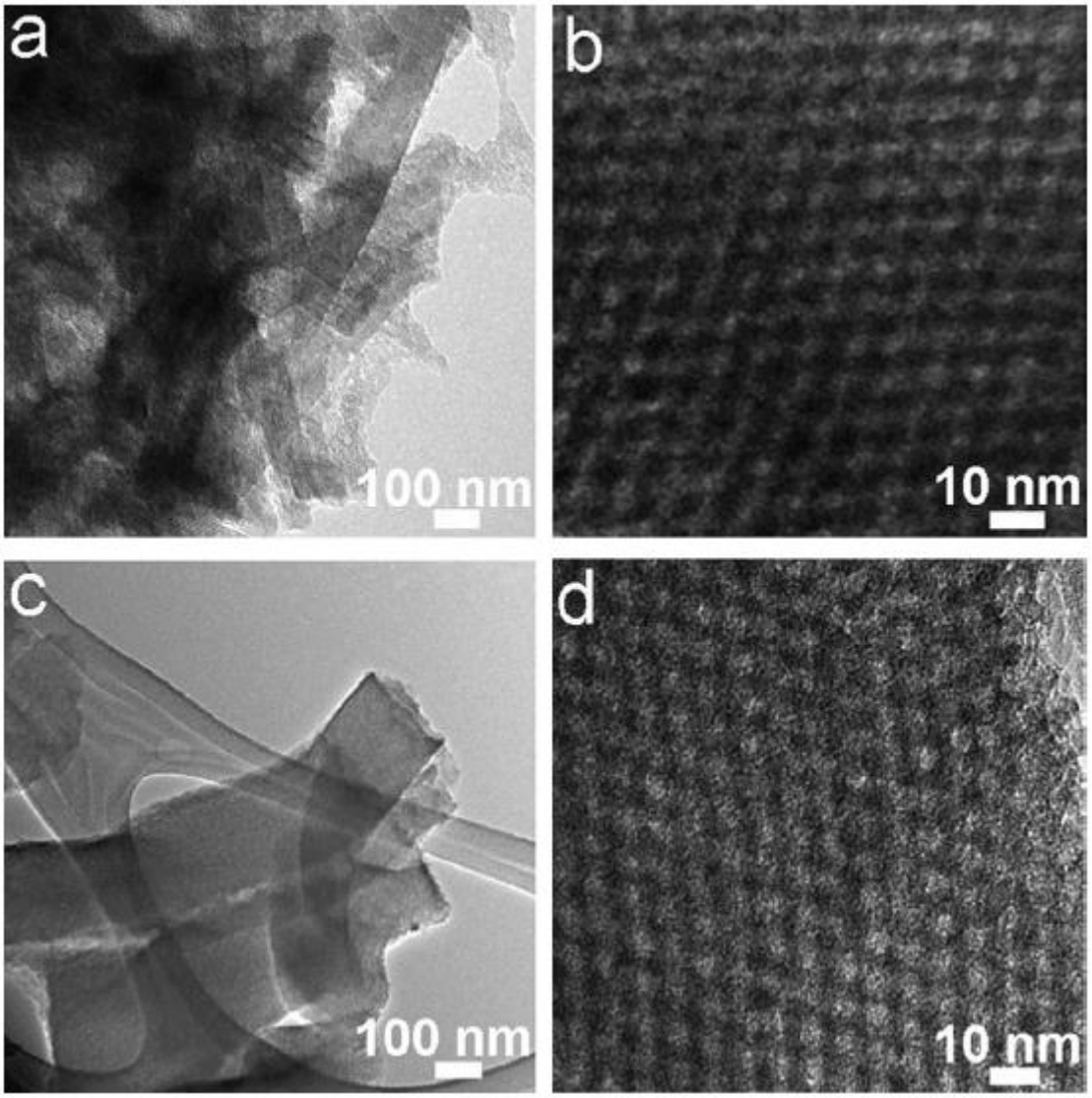

Figure 2

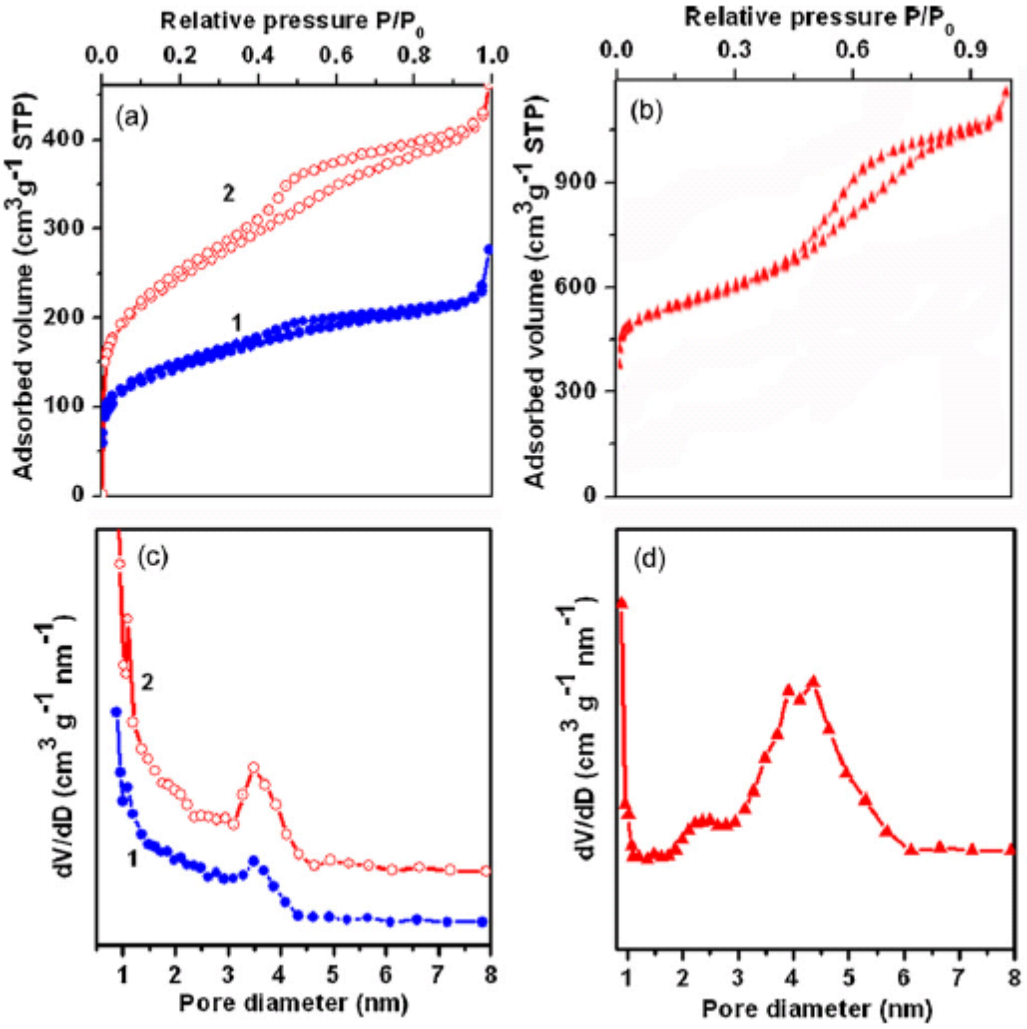
Relative pressure P/P0
0.0
0.2
0.4
0.6
0.8
1.0
(a)
Adsorbed volume (cm3g-1 STP)
0
100
200
300
400
2
1
Relative pressure P/P0
0.0
0.3
0.6
0.9
(b)
Adsorbed volume (cm3g-1 STP)
0
300
600
900
(c)
dV/dD (cm3 g-1 nm-1)
2
1
1
2
3
4
5
6
7
8
Pore diameter (nm)
(d)
dV/dD (cm3 g-1 nm-1)
1
2
3
4
5
6
7
8
Pore diameter (nm)

Figure 3

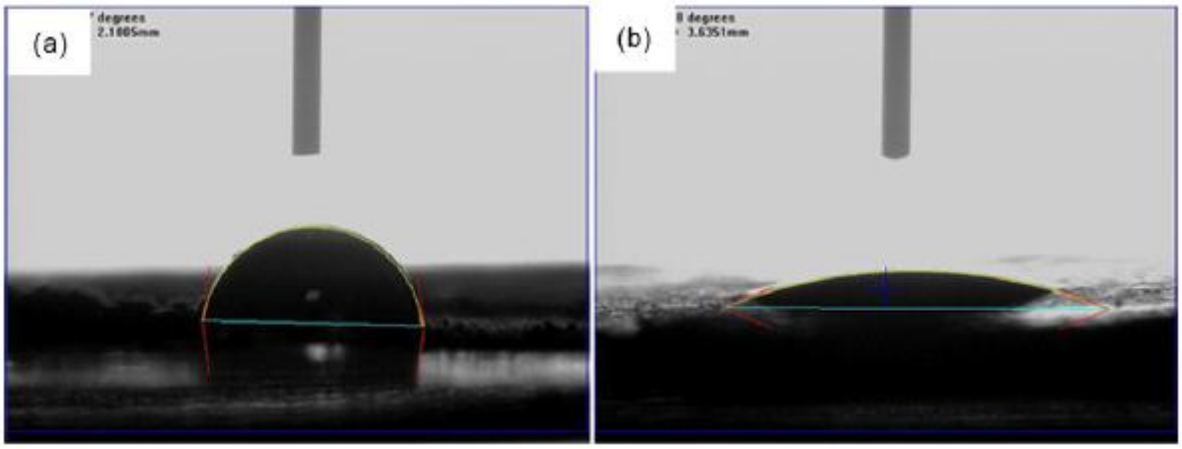

Figure 4

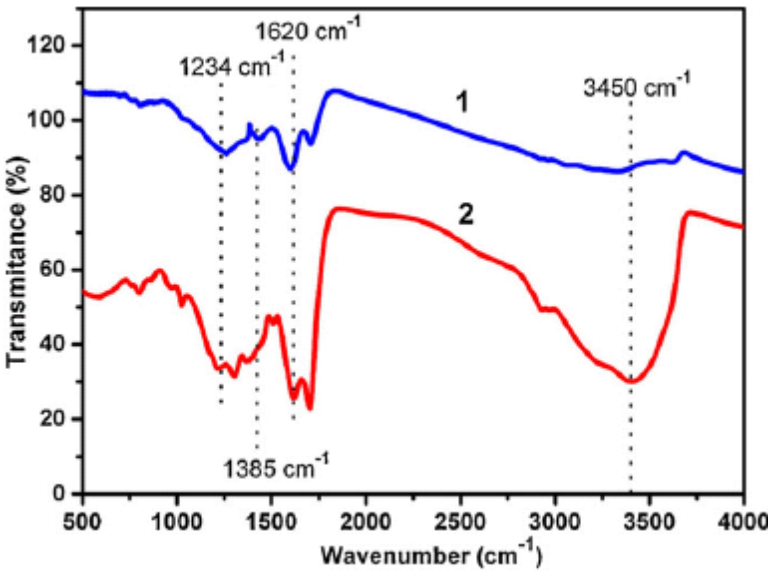
1620 cm-1
1234 cm-1
3450 cm-1
1
2
1385 cm-1
Transmitance (%)
Wavenumber (cm-1)
0
20
40
60
80
100
120
500
1000
1500
2000
2500
3000
3500
4000

Figure 5

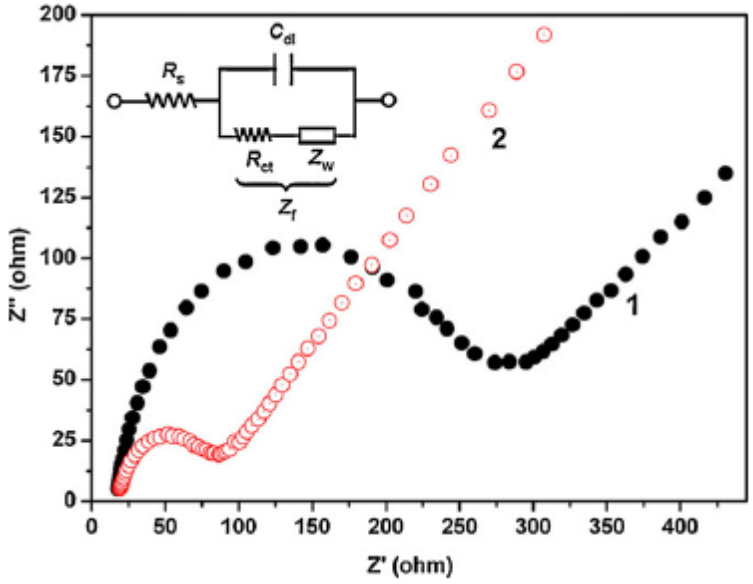
C_{dl}
R_s
R_{ct}
Z_w
Z_f
2
1
Z'' (ohm)
Z' (ohm)
0
25
50
75
100
125
150
175
200
0
50
100
150
200
250
300
350
400

Figure 6

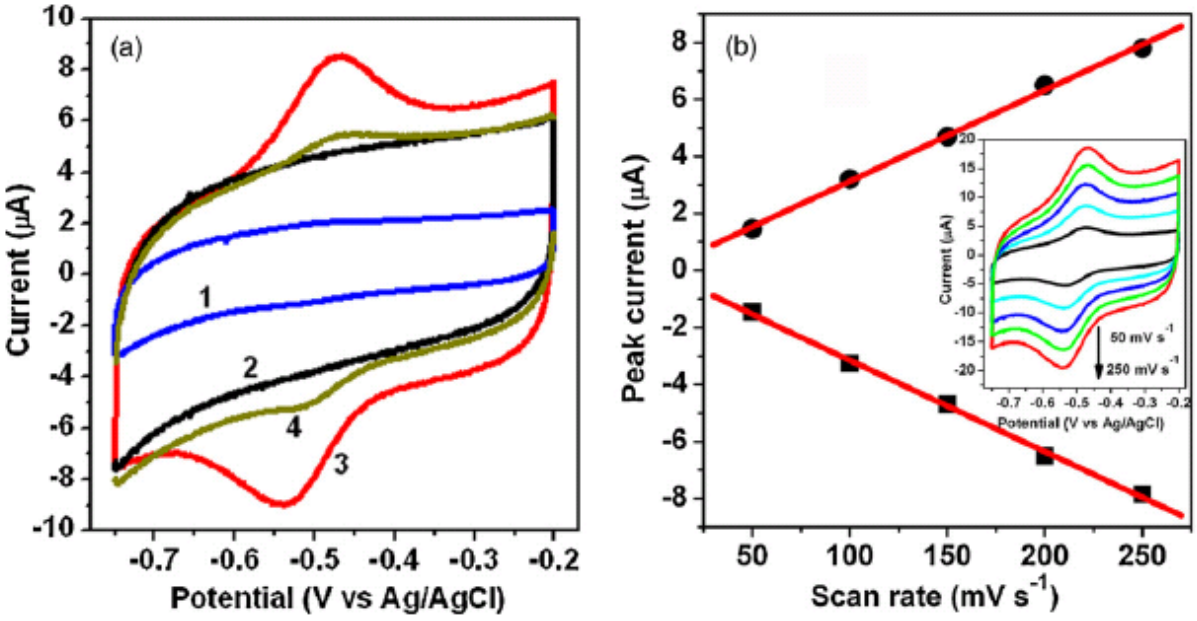
(a)
Current (μA)
Potential (V vs Ag/AgCl)
1
2
3
4
(b)
Peak current (μA)
Scan rate (mV s-1)
Current (μA)
Potential (V vs Ag/AgCl)
50 mV s-1
250 mV s-1

Figure 7

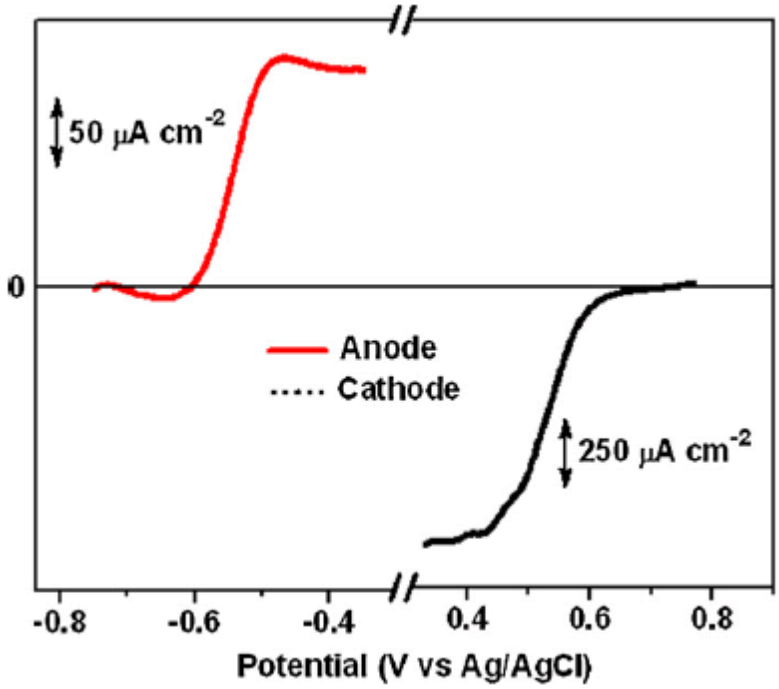
50 μA cm-2
0
Anode
Cathode
250 μA cm-2
-0.8
-0.6
-0.4
0.4
0.6
0.8
Potential (V vs Ag/AgCl)

Figure 8

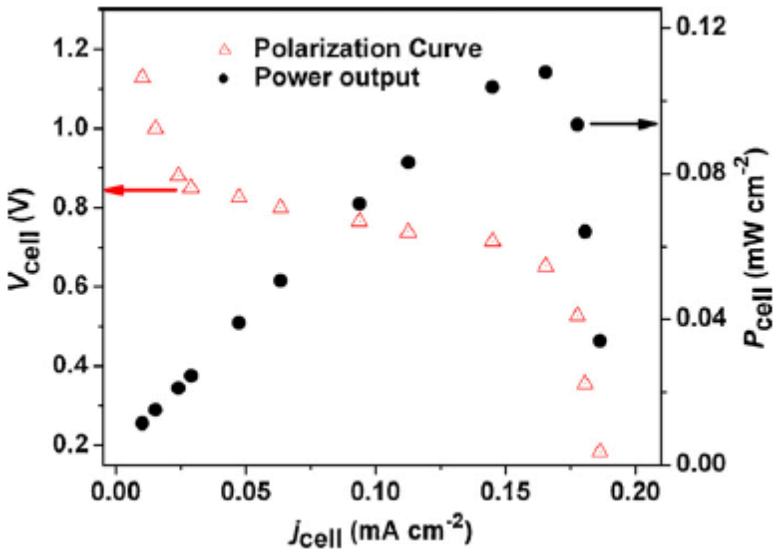
Polarization Curve
Power output
1.2
1.0
0.8
0.6
0.4
0.2
0.12
0.08
0.04
0.00
0.00
0.05
0.10
0.15
0.20
V_{cell} (V)
P_{cell} (mW cm^{-2})
j_{cell} (mA cm^{-2})

Figure 9

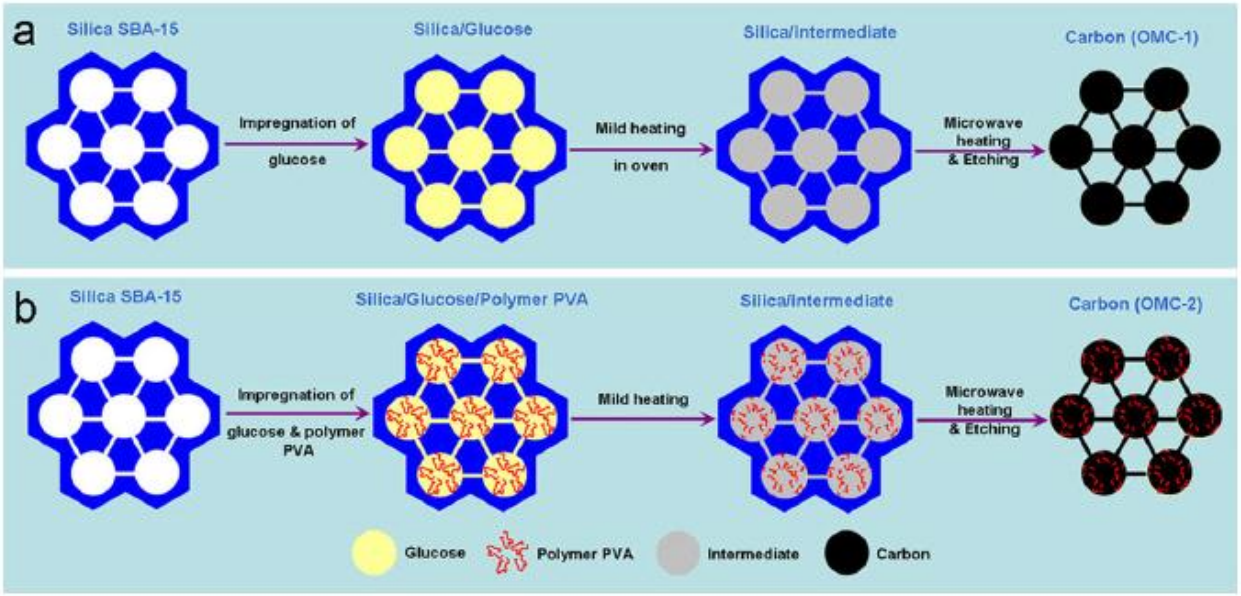
a
Silica SBA-15
Silica/Glucose
Silica/Intermediate
Carbon (OMC-1)
Impregnation of
glucose
Mild heating
in oven
Microwave
heating
& Etching
b
Silica SBA-15
Silica/Glucose/Polymer PVA
Silica/Intermediate
Carbon (OMC-2)
Impregnation of
glucose & polymer
PVA
Mild heating
Microwave
heating
& Etching
Glucose
Polymer PVA
Intermediate
Carbon

Scheme 1